Biochimica et Biophysica Acta 1820 (2012) 1–8

Contents lists available at SciVerse ScienceDirect

Biochimica et Biophysica Acta

journal homepage: www.elsevier.com/locate/bbagen

Effects of resveratrol on HepG2 cells as revealed by ^{1}H-NMR based metabolic profiling

Mara Massimi [a], Alberta Tomassini [b], Fabio Sciubba [b], Anatoli P. Sobolev [c], Laura Conti Devirgiliis [d], Alfredo Miccheli [b,*]

[a] Department of Basic and Applied Biology, University of L'Aquila, Via Vetoio, 67100 L'Aquila, Italy
[b] Department of Chemistry, Sapienza University of Rome, P.le Aldo Moro 5, 00185 Rome, Italy
[c] Istituto di Metodologie Chimiche, Laboratorio di Risonanza Magnetica "Annalaura Segre" - CNR, 00015, Monterotondo, Rome, Italy
[d] Department of Biology and Biotechnologies "Charles Darwin", Sapienza University of Rome, P.le Aldo Moro 5, 00185 Rome, Italy

ARTICLE INFO

Article history:
Received 18 July 2011
Received in revised form 4 October 2011
Accepted 11 October 2011
Available online 18 October 2011

Keywords:
Resveratrol
HepG2
Sirt1
Metabolic profiling
NMR spectroscopy
Metabolomics

ABSTRACT

Background: Resveratrol, a polyphenol found in plant products, has been shown to regulate many cellular processes and to display multiple protective and therapeutic effects. Several *in vitro* and *in vivo* studies have demonstrated the influence of resveratrol on multiple intracellular targets that may regulate metabolic homeostasis.
Methods: We analysed the metabolic modifications induced by resveratrol treatment in a human hepatoblastoma line, HepG2 cells, using a ^{1}H-NMR spectroscopy-based metabolomics approach that allows the simultaneous screening of multiple metabolic pathways.
Results: Results demonstrated that cells cultured in the presence or absence of resveratrol displayed different metabolic profiles: the treatment induced a decreased utilisation of glucose and amino acids for purposes of energy production and synthesis associated to a decreased release of lactate in the culture medium and an increase in succinate utilisation. At the same time, resveratrol treatment slowed the cell cycle in the S phase without inducing apoptosis, and increased Sirt1 expression, also affecting its intracellular localisation.
Conclusions: Our results show that the metabolomic analysis of the exometabolome of resveratrol-treated HepG2 cells indicates a metabolic switch from glucose and amino acid utilisation to fat utilisation for the production of energy, and seem in agreement with an effect mediated *via* AMPK- and Sirt1-activation.
General significance: NMR-based metabolomics has been applied in a hepatocyte cell culture model in relation to resveratrol treatment; such an approach could be transferred to evaluate the effects of nutritional compounds with health impact.

1. Introduction

Resveratrol (3,5,4′-trihydroxystilbene) is a polyphenol found in grapes, grape products and other plant products that has been the subject of intense scientific interest in recent years on account of its multiple protective and therapeutic effects [1–5]. Reported health benefits include cardioprotection, antiaging effects, defence against metabolic and neurodegenerative diseases, cancer prevention and therapy [6,7]. Some important cellular processes, such as cell cycle regulation and apoptosis are deeply influenced by this compound and its preventive and/or therapeutic properties against cancer have often been ascribed to antiproliferative and pro-apoptotic effects [8].

More recent research on the molecular mechanisms by which resveratrol might exert many of its biological effects has emphasised the importance of its interaction with sirtuins. In particular, resveratrol has been shown to increase Sirt1 activity and to enhance Sirt1-dependent metabolic processes both *in vivo* and *in vitro* [9–11].

Resveratrol can affect different metabolic pathways depending on the organ or cell type, on the cell state, and on the duration and dosage of treatment. At the same time, it has been shown that resveratrol has numerous intracellular targets and affects the expression and activity of different transcription factors/cofactors, thus regulating metabolic homeostasis and resulting in multiple pleiotropic effects. Among the numerous metabolic effects exhibited by resveratrol, the topic of "calorie restriction mimicry" has aroused considerable interest and several studies on cell cultures have been performed forcing the system toward either a fed or a fasted condition by increasing or decreasing nutritional supplies in the culture medium [10,12–14].

These considerations prompted us to study the metabolic modifications induced by resveratrol treatment in an *in vitro* system, using a metabolomic approach that allows the simultaneous screening of multiple metabolic pathways. Considering that the liver is one of

* Corresponding author at: Dipartimento di Chimica, Sapienza Università di Roma, P.le Aldo Moro 5, 00185 Rome, Italy. Tel.: +39 0649693270; fax: +39 0649913124.
E-mail address: alfredo.miccheli@uniroma1.it (A. Miccheli).

0304-4165/$ – see front matter © 2011 Elsevier B.V. All rights reserved.
doi:10.1016/j.bbagen.2011.10.005

the main target organs of resveratrol action *in vivo*, we analysed the effects of resveratrol on HepG2 cells, a human hepatoblastoma line that, although actively proliferating, exhibits many features specific to human differentiated hepatocytes, and is also widely used in resveratrol metabolic studies [15–17].

We first verified in our experimental conditions whether cellular responses to the treatment were similar to those reported in the literature, particularly in regard to antiproliferative and apoptotic effects [17,18]. Next, we studied the metabolic profile in relation to resveratrol treatment. Changes in the exo-metabolome were evaluated using ^{1}H-NMR spectroscopy on medium and Multivariate Data Analysis (MVDA). The utilisation of substrates and the concurrent release of metabolites into the extracellular space reflect the metabolic pathways that operate during a given set of physiological activities and in response to metabolic perturbations, either chemical or physical, leading to the characterisation of a specific metabolic profile (or fingerprint). Previously, this approach allowed us to discriminate two different metabolic profiles in HepG2 cells in relation to different phases of cell growth [19].

2. Materials and methods

2.1. Cell culture and viability

Human HepG2 cells were purchased from the American Type Culture Collection (ATCC) and were used within twenty passages. Cells, suspended in RPMI 1640 medium (Sigma) supplemented with 10% foetal calf serum, 2 mM L-glutamine, 1% sodium pyruvate, 100 μg/mL streptomycin and 100 U/mL penicillin, were seeded in culture plates at 8×10^{4} cells/cm^{2} at 37 °C in a humidified incubator in the presence of 5% CO_2. Resveratrol (Sigma), 20–200 μM in DMSO, was added to the cells and cultures were incubated for 24 or 48 h. Cells cultured in medium containing only DMSO were used as controls. At each time point, viable cells were estimated by a Trypan blue exclusion test. To evaluate the percentage of damaged cells, LDH leakage was monitored using an LDH Cytotoxicity Assay Kit (BioVision Inc.) on cells cultured in multiwells in the presence or absence of different amounts of resveratrol. DO was measured at 450 nm with a microplate reader (Bio-RAD).

2.2. Cytofluorimetric assay and DAPI staining

HepG2 cells after 24 or 48 h of treatment and control cells were extensively washed with PBS and 1×10^{6} aliquots were permeabilised with cold 70% ethanol for 30 min. The cells were then treated in the dark at room temperature with a DNA-staining solution (50 μg/ml propidium iodide in 0.1% sodium citrate containing 0.1% Triton X100). Cell cycle phase distribution was analysed by flow cytometry (FACScan flow cytometry, Becton Dickinson Immunocytometry System). Data from 10,000 events per sample were collected and analysed using Cell Quest software.

In parallel experiments, cells were cultured on coverslips and stained with DAPI (Sigma), 1:10,000 in PBS and observed under an epifluorescence microscope (Axioplan 2, Zeiss).

2.3. Sirt1 detection

2.3.1. Western blot analysis

To prepare the whole-cell lysates, cells were washed with ice-cold PBS, harvested and sonicated in lysis buffer (PBS containing 100 μg/mL PMSF and 5 μg/mL leupeptin). Proteins (80 μg) were separated on 10% SDS-PAGE and then transferred to a nitrocellulose membrane (Bio-Rad). The membrane was first blocked with 5% non-fat milk and then blotted with a rabbit polyclonal antibody to Sirt1 (Sigma) diluted 1:500 in Tris-bufferd saline (10 mM Tris–HCl, 150 mM NaCl, pH 7.4) for 2 h. After washing, the membranes were incubated with an anti-rabbit secondary antibody (1:10,000) for 1 h. The immunocomplexes were visualised by NBT-BCIP detection of alkaline phosphatase-conjugated secondary antibodies (Sigma). Quantitative analysis of the bands was performed on digitised images using the ImageJ 3.0 software. β-actin protein levels were determined to normalise the data.

2.3.2. Immunofluorescence

Cells grown on coverslips were fixed in methanol for 10 min at −20 °C, and non-specific staining was blocked with 10% normal goat serum in PBS. Cells were then incubated for 2 h at room temperature with a polyclonal antibody to Sirt1 (Sigma), 1:80 in PBS with 1% BSA. They were then stained with Alexa Fluor 555-conjugated goat anti-rabbit IgG for 1 h at room temperature (Molecular Probes, Invitrogen). After rinsing, the coverslips were mounted on slides in aqueous medium and examined under an epifluorescence microscope (Axioplan 2, Zeiss). Negative controls were performed by exposing slides under similar conditions while omitting the primary antibody.

2.4. Oil Red O staining

Cells were fixed in 10% formaldehyde in PBS for 1 h (or overnight) and stained with a working solution (5 mM) of Oil Red O (Sigma) for 10 min at room temperature. For quantitative analysis of cellular triglycerides, after exhaustive washings with water samples were dried and 60% isopropyl alcohol was added. The extracted dye was immediately removed by gentle pipetting and its absorbance was monitored by a spectrophotometer (Genesys) at 500 nm.

2.5. ^{1}H NMR spectroscopy and multivariate analysis

2.5.1. ^{1}H NMR spectroscopy

^{1}H NMR Spectra were acquired at a temperature of 298 K using a Bruker Avance 400 spectrometer (Bruker BioSpin GmbH, Germany) equipped with a magnet operating at 9.4 T, where the ^{1}H nucleus resonates at 400.13 MHz. The probehead was a 5 mm diameter multinuclear PABBO BB-1H/D (Z108618/0044) equipped with z-gradient. The pulse sequence adopted for spectra acquisition was a presaturation–single 90° detection pulse–acquire–delay sequence that is a modification of the presaturation ZGPR sequence available as a standard sequence in the spectrometer library. The modification makes it possible to set the presaturation delay independently of the D1 relaxation delay, while in the standard sequence the solvent signal is saturated for the entire duration of the relaxation delay. Since our spectra were acquired under full relaxation conditions, with a very long relaxation interval (9.5 s), our sequence allowed us to irradiate the solvent nuclei for a given time (3 s) leaving a true relaxation delay of 6.5 s. The acquisition time needed to collect the 32 K points was about 5.5 s, allowing proton nuclei other than solvent nuclei to relax for 15 s, complying with the full relaxation condition after a 90° pulse. The duration of the detection pulse was calibrated prior to the acquisition of each spectrum, the spectral width was set to 5995.02 Hz (12 ppm), 64 scans were collected for each spectrum. 1H NMR spectra were processed using the 1H-Manager ver. 12.0 software (Advanced Chemistry Development, Inc., Toronto, Ontario, Canada). The assignment of peaks to specific metabolites was achieved using an internal library of compounds and the literature [20,21, www.hmdb.ca] and confirmed by standard two-dimensional (2D) ^{1}H–^{1}H correlation spectroscopy (COSY), total correlation spectroscopy (TOCSY), and ^{1}H–^{13}C heteronuclear single quantum correlation (HSQC).

2.5.2. Multivariate analysis

Multivariate data analysis was carried out using Unscrambler 9.8 Software (CAMO, Oslo, Norway). Spectral data were mean centred and scaled before analysis [22] Principal components analysis (PCA) was used to examine inherent clustering and to identify outliers.

In addition, Projection to Latent Structure (PLS) or Partial least squares-discriminant analysis (PLS-DA) [22] methods were applied to maximise the distinction between sample groups, focusing on differences according to group metabolic variations, and to assess the correlation between the observed NMR data and class membership information (i.e. an external variable that indicates to which class the samples belong, of which the values are 0 for control and 1 for resveratrol-treated samples) as the response variable. Unpaired Student's *t*-test was applied to the discriminant variables obtained from partial least squares discriminant analysis; a P value <0.05 was considered significant.

2.6. ^{13}C NMR spectroscopy

A serum-free RPMI 1640 medium supplemented with ITS (Sigma-Aldrich), 1% BSA (Fluka, BioChemika, Germany), 0.1 μM dexamethasone, 3.7 g/L $NaHCO_3$, 5.5 mM glucose, 0.5 mM carnitine, 0.5 mM [U-$^{13}C_{18}$] oleate (Isotec) was used for labelled oleate experiments.

^{13}C-NMR spectra of cell and medium extracts were obtained on a Bruker Avance 600 spectrometer (Bruker Spectrospin, Milano, Italy) operating at 600 MHz (^{1}H) and 150.9 MHz (^{13}C), respectively. Dried samples were dissolved in 500 μl of D_2O (hydrosoluble fraction). 30 μl of acetonitrile in an external capillary tube were used in ^{13}C spectra as a reference for chemical shifts and quantitative analysis. Proton decoupled ^{13}C spectra were acquired with the following parameters: 45° pulse, 31,000 Hz spectral width and 32K data points in time domain. The acquisition time was 0.52 s and an additional delay of 6.48 s was used to achieve fully relaxed conditions for each carbon resonance. To avoid Nuclear Overhauser Effect, ^{13}C spectra were ^{1}H decoupled only during acquisition using an inverse-gated sequence.

The NMR data were processed off-line using Topspin software (Bruker-Franzen Analitik GmbH, Bremen, Germany). Apodisation with 0.5 Hz exponential line broadening was used for ^{13}C spectra only.

Peak areas were used to quantify ^{13}C spectra. In ^{13}C spectra the total amount of ^{13}C in each carbon resonance of a specific metabolite was determined using acetonitrile as a standard reference. Fractional ^{13}C enrichment was calculated for each carbon atom using the formula: $([^{13}C]_t - [^{13}C]_a) \times 100/[m]$, where $[^{13}C]_t$ was the total quantity of ^{13}C; $[^{13}C]_a$ was the natural abundance of ^{13}C (1.1%) and [m] was the total quantity of the relevant metabolite [23]. The concentration of glutamate was measured from ^{13}C singlet resonance at 182.8 ppm. The levels of [4,5-$^{13}C_2$] glutamate isotopomer were measured by the area of the doublet at 182.8 ppm. The synthesis of C_4–C_5 glutamate ^{13}C isotopomer is related to production of [1,2-$^{13}C_2$] Acetyl-CoA from [U-$^{13}C_{18}$] oleate through the beta-oxidation, as reported in Fig. 1. The U–Mann Whitney non parametric statistical test has been applied to the data to evaluate the significance of the observed differences on three independent experiments.

3. Results

3.1. Effects of resveratrol treatment on cell cycle, apoptosis and Sirt1 expression

We first investigated in our experimental system the effects of resveratrol on proliferation, apoptosis and Sirt1 expression and localisation, in order to choose the best conditions for the metabolomic analysis. Cells were plated and cultured to high density and then treated with 20–200 μM resveratrol for 24 or 48 h. The decrease of cell growth was dose- and time-dependent, with an apparent GI50 of 80 μM and 40 μM after 24 and 48 h of culture, respectively. Treatment with resveratrol resulted in a decreased cell number with respect to controls: this effect was not due to cytotoxicity of the drug when the concentration of 40 μM was used, as demonstrated by the LDH leakage test (Fig. 2) and Trypan Blue exclusion test. At this resveratrol concentration the percentage of dead cells was only about 5% at both 24 h and 48 h and was similar to that obtained in the controls. This concentration was thus used for the subsequent experiments.

Cytofluorimetric assays indicated the influence of resveratrol on the cell cycle: the treatment caused a decrease in cell numbers in both the G1 and G2 phases of the cell cycle, while cells accumulated in the S phase (Fig. 3 A, B), suggesting a resveratrol-induced blockade or slowing of the cell cycle. At the same time, neither hypoploid peaks nor pictures of DNA fragmentation after DAPI staining (Fig. 3 C) were detectable. In fact, the nuclei from control and treated cells appeared similarly stained with the fluorescent dye, and the sporadic occurrence of pictures of chromatin fragmentation was not dependent on resveratrol treatment, excluding cell death by an apoptotic mechanism. Western blot experiments were carried out to evaluate Sirt1 levels after resveratrol treatment. The results showed a 30% increase in Sirt1 expression in treated cells compared with controls, after both 24 h and 48 h (Fig. 4 A). When immunolocalization of Sirt 1 was performed, a different localization of this protein was observed (Fig. 4). Staining was well visible in the cytoplasm of both control and treated cells. However, in treated cells, the positivity appeared to be increased in the nuclei; this effect was marked after 48 h of treatment (Fig. 4d arrows). This indicates a resveratrol-induced nuclear translocation of Sirt-1, which takes up a position more suitable to its function.

Finally, a quantitative evaluation of total triglycerides in treated and untreated cells was performed using the oil red O test. Results, expressed as arbitrary OD units, were similar after 24 h of treatment (Control 24 h: 202 ± 10.1; Resveratrol 24 h: 200 ± 11.3) while a 20%

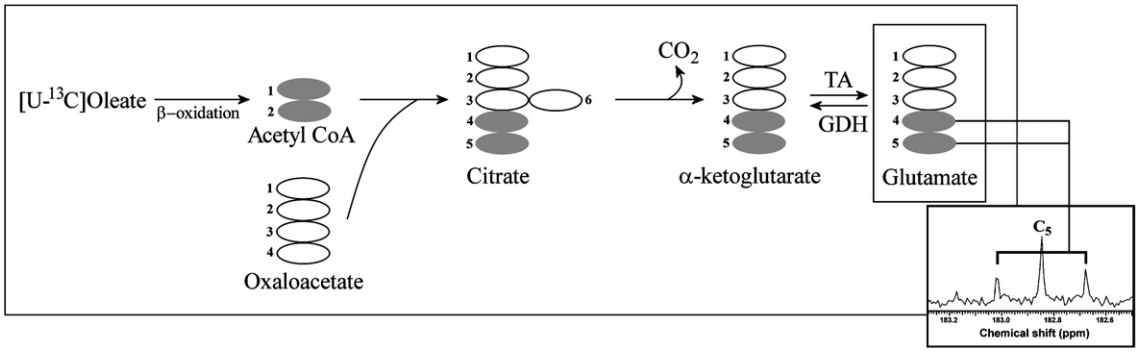

Fig. 1. The pathway of synthesis of C_4–C_5 glutamate ^{13}C isotopomer in TCA cycle from [1,2-$^{13}C_2$] Acetyl-CoA produced through [U-$^{13}C_{18}$] oleate beta-oxidation is described. In grey: ^{13}C labelled carbons. In the separated box, the ^{13}C signals of glutamate, namely C5 and relative C4–C5 coupling, utilised for enrichment measurements are reported.

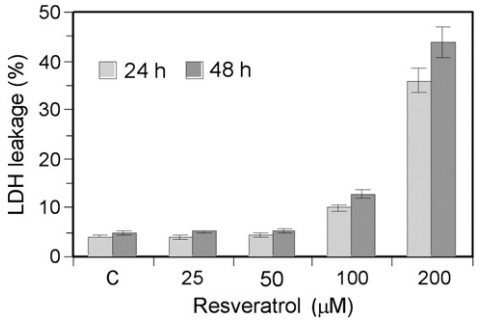

Fig. 2. LDH leakage test. Effect of different concentrations of resveratrol on LDH leakage after 24 h and 48 h of treatment. Results are the means of three independent experiments ± SE. The percentage of damaged cells was similar to that obtained in the controls up to 50 μM.

decrease was observed after 48 h (Control 48 h: 203 ± 10.2; Resveratrol 48 h: 160 ± 9.4).

3.2. ^{1}H- and ^{13}C-NMR spectroscopy

Table 1 shows the chemical shifts and multiplicity of resonances of the metabolites present in the samples of RPMI culture medium after 48 h. The concentrations of the assigned metabolites, measured by the integrated area of the resonances (reported in supplementary data), are expressed as differences between the levels at the beginning and at the end of the experimental time and are normalised for cell numbers (Fig. 5A and B). Thus the data are representative of net balances, with positive and negative values being considered as an estimate of net fluxes of production and utilisation of metabolites, respectively. Both in control and treated cells the utilisation of branched amino acids (isoleucine, valine) and other amino acids such as glutamine, phenylalanine, histidine and tyrosine was determined. Glucose, pyruvate and succinate were also consumed during the experiment. Conversely, positive delta values were observed for alanine, glutamate, ornithine, lysine, glycine, threonine, formate and lactate, as well as for the ketoacids related to the utilised branched amino acids, such as 2-oxo-3-methyl-valerate, 2-oxo-isovalerate and 3-hydroxy-isobutyrate which are released in the culture media (Fig. 5A and B).

Statistically significant variations in net balances of metabolites were found only for some compounds; resveratrol-treated cells used less valine ($p<0.005$), isoleucine ($p<0.01$) and tyrosine ($p<0.05$) while only 3-hydroxy-isobutyrate levels resulted significantly increased ($p<0.05$). Interestingly, a statistically significant reduced utilisation of glucose ($p<0.005$) was paralleled by a statistically significant reduced production of lactate ($p<0.005$). Finally, resveratrol treatment caused higher succinate utilisation ($p<0.001$). Neither glutamate production, nor glutamine utilisation were significantly different in control and treated culture media.

On the basis of the results obtained, suggesting a decreased glycolytic activity and decreased amino acid utilisation for energy purposes, we hypothised a resveratrol-dependent activation of different metabolic processes to produce energy. To verify this point we used ^{13}C-NMR spectroscopy to study fatty acid utilisation by adding [U-$^{13}C_{18}$] oleate to the medium of control and resveratrol-treated cultures. It is possible to obtain information on the metabolic processes involved in oleate utilisation by analysing the isotopomer distribution of the ^{13}C labelling in different metabolites.

From the labelling of C4 and C5 carbon atoms of glutamate we calculated the contribution of acetyl-CoA, produced through the mitochondrial beta oxidation of oleate, to the Krebs cycle in the synthesis of ketoglutarate. Percentage fractional enrichments of glutamate C4–C5 carbon atoms were 4.2 ± 0.4 and 5.2 ± 0.5 ($p<0.05$) in the control and treated cultures, respectively. The results showed a 20% resveratrol-dependent increase in mitochondrial beta-oxidation compared with controls.

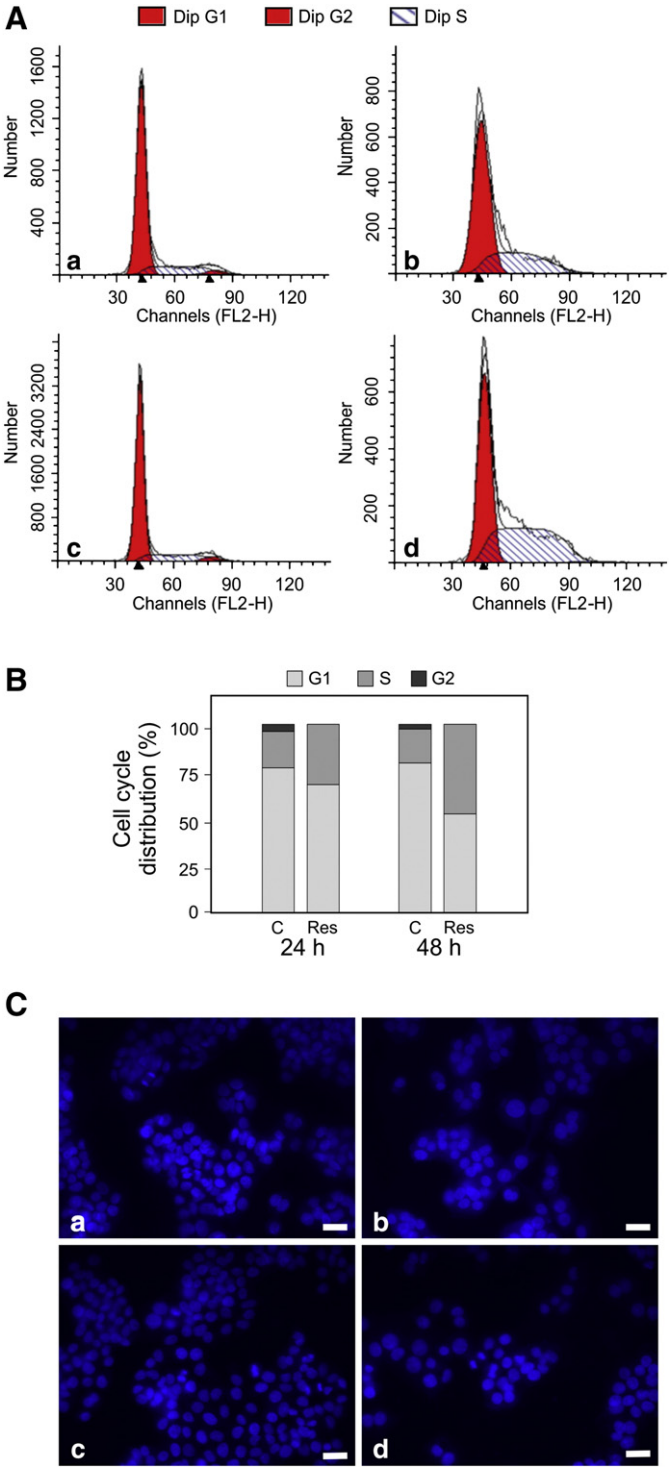

Fig. 3. Resveratrol effects on cell cycle distribution and apoptosis. (A) Representative experiment of resveratrol effects on cell cycle distribution of HepG2 cells evaluated by Flow Cytometry after PI staining of nuclei. Cells were incubated for 24 h (b) or 48 h (d) with 40 μM resveratrol, which was omitted in controls (a, c). An increase in cell numbers in S phase paralleled with a decrease in G1/G2 phases was evident in treated cells. (B) Histograms of cell cycle distribution of control and 40 μM resveratrol treated HepG2 cells. Data are expressed as percentages of the total cell population in each cell cycle phase, means of three independent experiments. (C) DAPI nuclear staining of control (a, c) and 40 μM resveratrol treated (b, d) HepG2 cells at 24 h (a,b) and 48 h (c,d). Nuclei with a condensed and fragmented morphology were completely absent, excluding a resveratrol-induced apoptosis (Bars = 20 μm).

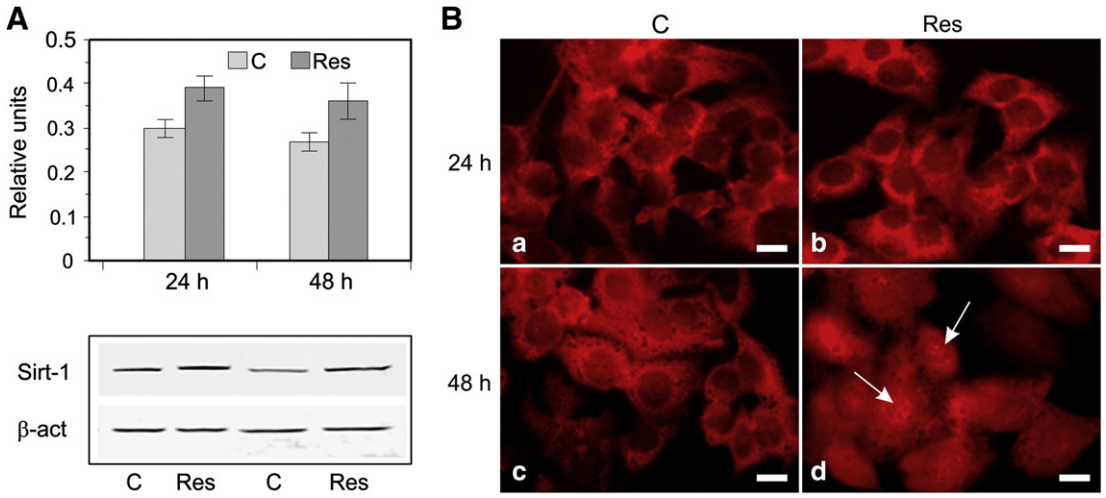

Fig. 4. Sirt 1 expression and localisation. (A) Representative Western blot of Sirt1 levels after 24 h and 48 h of 40 μM resveratrol treatment. Histograms show the densitometric values expressed as arbitrary units. Beta-actin levels were used to normalise results. Data are the means ± S.E. of three independent experiments performed in duplicate. Statistical significance was determined using Student's *t*-test. A significant resveratrol dependent increase in Sirt1 ($P<0.01$) was shown at both times of treatment. (B) Immunofluorescence localisation of Sirt1 in control HepG2 cells (a, c) and at 24 h (b) and 48 h (d) of 40 μM resveratrol treatment. The positivity, represented by a uniform red colour in the pictures, was well visible in the cytoplasm of both control and treated cells. A nuclear localisation was evident in treated cells after 48 h of treatment (arrows). Bars = 10 μm.

3.3. Metabolic profiling and multivariate analysis

Principal Components Analysis was applied to the data set using metabolite net balances obtained from control and resveratrol-treated cultures in order to explore the data field. Resveratrol-treated samples were clearly discriminated from controls by PLS analysis (Fig. 6). The PLS discriminant model was validated and found to be predictive ($R^2 = 0.958$, $Q^2 = 0.828$).

The significant discriminant metabolites in the PLS analysis were valine, isoleucine, lactate, succinate, glutamine, ornithine, glucose, tyrosine, hystidine and phenylalanine (Table 2). As a positive regression value for utilised metabolites means an increased level in the medium, valine, isoleucine, glutamine, glucose and tyrosine resulted less utilised by the treated cells. Resveratrol-treated cells were also found to consume more succinate, as shown by the negative regression sign in the PLS analysis analogously to histidine and phenylalanine. Finally, the regression sign for lactate and ornithine was negative, indicating that they were produced in smaller quantities.

In order to acquire additional information on the biological significance of the observed variations, we analysed the correlation matrices from the pair-wise linear Pearson's correlations in each experimental group. A relevant variation in connectivity was observed among net balances of the discriminating metabolites in the correlation matrix. In particular, succinate, which did not show any significant correlation in control cultures, acquired a positive Pearson's correlation with lactate in the resveratrol-treated cultures ($R^2 = 0.854$). As succinate is utilised and lactate is produced, a positive correlation means that when more succinate is used, less lactate is produced, as shown in resveratrol-treated cultures.

4. Discussion

Resveratrol has been shown to influence several metabolic pathways in both *in vivo* and *in vitro* experimental systems, creating great interest in applications that could be useful for human health. We focused on energy metabolism, since this molecule exerts an effect that mimics calorie restriction [1,12,24].

Many different molecular mechanisms of action have been shown to influence cell metabolism with a long list of involved up or down regulated target genes and activated or suppressed factors/cofactors. Resveratrol treatment increases insulin sensitivity, AMPK and PGC-1α activity, and mitochondrial numbers, while it reduces insulin-like growth factor-1 (IGF-1) levels and inhibits AKT/PBK phosphorylation involved in glucose uptake and metabolism [25,26].

In this context, it is not surprising that the pleiotropic effects of resveratrol are reflected in a variety of different outcomes that are strictly dependent on cell type or organ and on experimental conditions, as well as on dose and treatment.

To investigate the metabolic system affected by resveratrol treatment, we applied an NMR-based metabolomics approach to test whether it was possible to discriminate different metabolic profiles in an *in vitro* model, depending on treatment. In particular, we studied changes in the exometabolome, given that substrate utilisation and production and substrate flux distribution reflect the cell's physiological state and thus its metabolome [19,27].

The metabolic profile of the high density control cultures, that is characterised by glucose, pyruvate and succinate utilisation and lactate, alanine and keto-acids production, and the cell cycle phase distribution were both in agreement with our preceding data [19].

We studied the global metabolic effect of treatment using a 40 μM resveratrol concentration in confluent cultures at an experimental time of 48 h; this dose, which represented the GI_{50} at 48 h of treatment, caused neither necrosis nor apoptosis. At the same time, we demonstrated an accumulation of cells in the S phase of the cell cycle, together with a decrease in cells in G1 and G2. These results are in agreement with literature data showing a strong S-phase delay, a slowdown in cell cycle progression without an increase in apoptosis or necrosis [15,18,28]. In contrast, other authors, in addition to showing a blockade of proliferative activity, also found apoptotic effects of resveratrol on hepatoma cells. These discrepancies are probably associated with different experimental conditions [17,29,30].

The PLS multivariate analysis of the net balances of metabolites clearly showed a discrimination between control and resveratrol-treated cultures, characterised in the latter by a decreased glucose and amino acid utilisation for energy production, with succinate replenishing the Krebs cycle as an anaplerotic substrate. A recent metabolomic study showed that a resveratrol treatment induced an intracellular aminoacids increase associated to growth inhibition in human breast cancer cell lines [31]. An intracellular aminoacids increase could be explained by a decreased utilisation, in agreement with our data.

Glucose and lactate were among the discriminant metabolites with opposite sign; as glucose is consumed and lactate released, an opposite sign means that when glucose is less utilised, lactate is less

Table 1
Resonance assignations of metabolites identified in ^{1}H-NMR spectra of RPMI 1640 medium.

Molecule (abbreviation)	^{1}H chemical shifts (multiplicity)	Observed
Isoleucine (Ile)	0.93 (t) – 1.02 (d) – 1.27 (m) – 1.47 (m) – 2.00 (m) - 3.68 (m)	TOCSY, COSY
Leucine (Leu)	0.94 (d) – 0.97 (d) – 1.72 (m) – 3.74 (t)	TOCSY, COSY
Valine (Val)	0.99 (d) – 1.04 (d) – 2.26 (m) – 3.61 (d)	TOCSY, COSY
2-Oxo-3-methyl-n-valerate (2-OMV)	0.90 (d) – 1.10 (d) – 1.48 (m) – 1.71 (m) – 2.95 (m)	TOCSY
2-Oxo-isovalerate (2-OIV)	1.13 (d) – 3.04 (m)	TOCSY
3-OH butyric acid (3-OH But)	1.19 (d) – 4.48 (m)	TOCSY
Lactate (Lac)	1.32 (d) – 4.13 (q)	TOCSY, COSY
Threonine (Thr)	1.34 (d) – 3.54 (m) – 4.28 (m)	TOCSY, COSY
Alanine (Ala)	1.49 (d) – 3.78 (m)	TOCSY, COSY
Lysine (Lys)	1.47 (m) – 1.73 (m) – 1.91 (m) – 3.04 (t) – 3.78 (m)	TOCSY, COSY
U2	1.56 (dd) – 1.88 (m) – 3.15 (dd)	TOCSY
Ornithine (Orn)	1.78 (m) – 1.93 (m) – 3.05 (t) – 3.78 (t)	TOCSY, COSY
Acetate (Ace)	1.92 (s)	
Glutamate (Glu)	2.03 (m) – 2.35 (dt) – 3.77 (m)	TOCSY, COSY
Proline (Pro)	2.04 (m) – 2.35 (m) – 3.33 (t) – 3.43 (t) – 4.15 (t)	TOCSY, COSY
Glutamine (Gln)	2.13 (m) – 2.45 (dt) – 3.78 (m)	TOCSY, COSY
Pyruvate (Pyr)	2.38 (s)	
Succinate (Suc)	2.41 (s)	
U4	2.60 (s)	
Aspartate (Asp)	2.67 (dd) – 2.82 (dd) – 3.91 (dd)	TOCSY, COSY
Asparagine(Asn)	2.86 (dd) – 2.95 (dd) – 4,02 (m)	TOCSY, COSY
U5	3.11 (m) – 3.30 (m)	TOCSY, COSY
U6	3.20 (m) – 3.74 (m) – 3.90 (m)	TOCSY, COSY
Glucose β (Glc β)	3.26 (dd) – 3.40 (m) – 3.49 (m) – 3.74 (m) – 3.90 (m) – 4.66 (d)	TOCSY, COSY
Myo-inositol (Myo-ino)	3.29 (t) – 3.53(m) – 3.65 (m) – 4.08 (m)	TOCSY, COSY
Glucose α (Glc α)	3.42 (dd) – 3.55 (dd) – 3.73 (m) – 3.83 (m) – 5.25 (d)	TOCSY, COSY
Glycine (Gly)	3.56 s	
Serine (Ser)	3.84 (dd) – 4.12 (m)	TOCSY
U7	4.02 (d)	
Tyrosine (Tyr)	6.90 (d) – 7.20 (d)	TOCSY
Histidine (His)	7.06 (s) – 7.77 (s)	TOCSY
Phenylalanine (Phe)	7.36 (m) – 7.43 (m)	TOCSY
Formate (For)	8.46 (s)	TOCSY
Nicotinamide (Nad)	7.60 (m) – 8,25 (m) – 8,73 (m) – 8.95 (s)	TOCSY

Chemical shifts (ppm) are referred to trimethylsilylpropionate as internal standard; s, singlet; d, doublet; dd, double of doublets; t, triplet; dt, doublet of triplets; q, quartet; m, multiplet.

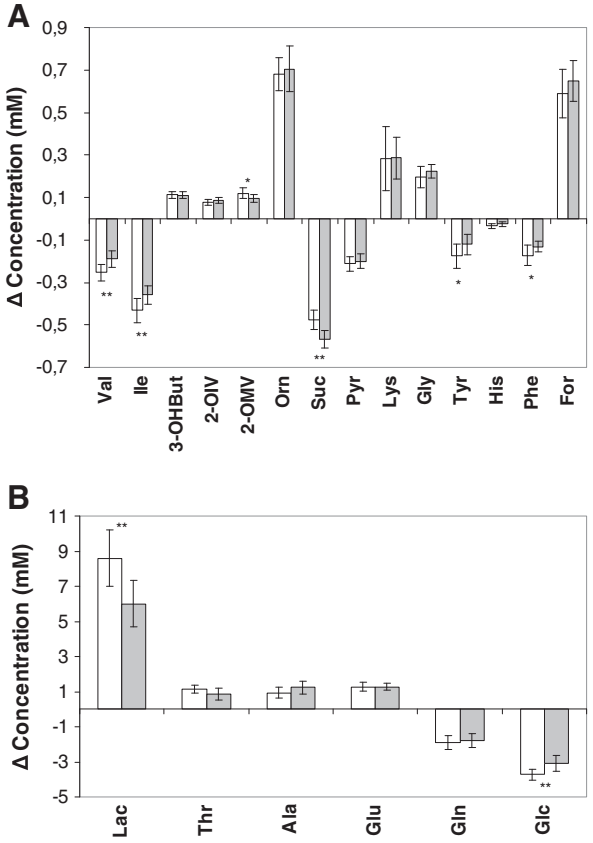

Fig. 5. Net balances of extracellular metabolites. Net balances of extracellular metabolites in control (empty bars) and resveratrol treated (full bars) samples. Balance concentrations were obtained subtracting medium metabolite levels at 48 h with the ones at 0 h. Data are expressed as means ± S.D. of nine independent experiments. Unpaired Student's *t* test: $P<0.05$ (*), $P<0.01$ (**).

produced, indicating a resveratrol induced decreased glycolytic activity. A resveratrol-induced mimicry of an energy-restricted state, characterised by a decreased glucose uptake and lactate production with suppression of AKT and mTOR signalling, was also observed in human ovarian cancer cells [32], although a decreased glucose uptake was not observed in large B cell lymphomas [33]. These differing results could be due to differences in glucose uptake and metabolism as well as to differences in glucose deprivation sensitivity among diverse cancer cell types and normal cells. In HepG2 cells a reversal of the effects of hyperglycaemia characterised by AMPK activation and increased lactate release through resveratrol treatment has been demonstrated. An increase in AMPK activity has also been observed, although after less time and at a much higher dose (100 μM) than in our experimental conditions [14]. Furthermore, resveratrol treatment has been shown to down-regulate glycolysis and to oppose the effects of high caloric intake in a mouse model [1].

In mammals, AMPK functions as a cellular energy sensor and glucose sensor [34,35]. In particular, AMPK phosphorylates and inactivates ACC2 (acetylcoenzyme A carboxylase-2), which produces malonyl-CoA; as the latter product is an inhibitor of fatty acid uptake by mitochondria *via* the carnitine palmitoyltransferase system, the final effect of AMPK activation is a stimulation of fatty acid oxidation. In agreement, our results showed an increase in ^{13}C-fractional enrichment in glutamate C4–C5 carbon atoms, suggesting a switch from

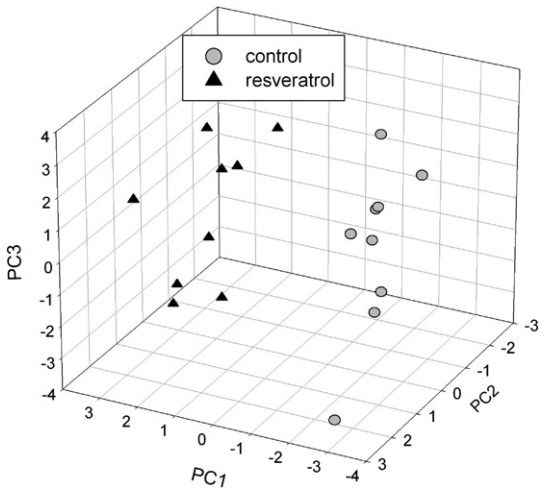

Fig. 6. PLS-DA score plot. PLS-DA score plot of control and resveratrol treated samples is shown. Y variance values for PC1, PC2 and PC3 were 80%, 9% and 3%, respectively. The PLS discriminant model was validated and found to be predictive ($R^2 = 0.958$, $Q^2 = 0.828$).

Table 2
PLS-DA analysis: significant metabolite balances in relation to resveratrol treatment.

Molecule (abbreviation)	Direction of regression	p-values (*t* test)	Metabolic change direction
Valine (Val)	↑	0.004	Decreased utilisation
Isoleucine (Ile)	↑	0.009	Decreased utilisation
Lactate (Lac)	↓	0.002	Decreased production
Succinate (Suc)	↓	0.001	Increased utilisation
Glutamine (Gln)	↑	n.s.	Decreased utilisation
Glucose (Glc)	↑	0.003	Decreased utilisation
Tyrosine (Tyr)	↑	0.014	Decreased utilisation
Phenylalanine (Phe)	↑	0.036	Decreased utilisation
Histidine (His)	↑	n.s.	Decreased utilisation

The significance of the regression coefficients of metabolite balances in relation to resveratrol treatment was calculated by applying the uncertainty test. p-values were calculated by unpaired Student's *t* test. The direction of metabolic changes was evaluated by comparison of metabolite net balance values. n.s. = not significant.

glycolysis to fatty acid β-oxidation. AMPK involvement was supported both by the increased expression of Sirt1 and by a resveratrol-dependent lowering of intracellular lipid content, as shown by the Oil-Red-O test. Our data are in agreement with findings that polyphenols reverse the effects of high glucose levels on AMPK phosphorylation and its downstream target ACC, FAS expression and lipid accumulation in HepG2 cells [10]. Furthermore, a crosstalk between the Sirt1 and FOXO1 pathways influencing SREBP1 expression in relation to resveratrol treatment has been demonstrated in HepG2 cells cultured in the presence of palmitate as a cell model of steatosis [13]. An interplay among the above pathways and an important metabolic regulator, PGC-1α has also been shown, suggesting that Sirt1 plays a critical role in regulating hepatic lipid metabolism and that treatment with Sirt1 activators such as resveratrol increases fatty acid oxidation and regulates fat synthesis and mitochondrial function [36–41].

Interestingly, a resveratrol-induced metabolic profile characterised by increased utilisation of succinate can be inferred from the PLS analysis. Recently, mass spectroscopic studies have revealed that numerous TCA cycle enzymes and fatty acid oxidation enzymes and subunits of oxidative phosphorylation complexes are modified by acetylation in response to metabolic stress [42]. In particular, Sirt3, which localised on the inner membrane of mitochondria and is highly expressed in the liver [43], has been shown to interact with several enzymes of the Krebs cycle, possibly regulating the flux through TCA [42,44,45]. An acetyl-CoA and/or NADH/NAD^+ ratio-dependent regulation through deacylation by Sirt3 of succinate dehydrogenase (SDH) activity has been demonstrated in wild-type mice [45]. SDH is an inner membrane-bound enzyme complex whose activity influences both the Krebs cycle and oxidative phosphorylation. The deacylation of SDH by a NAD^+-induced Sirt3 activation will promote the generation of NADH and FADH2 for ATP synthesis in a condition of nutrient deprivation [45]. Sirt3 also influences the TCA cycle by activating glutamate dehydrogenase (GDH) that regulates the aminoacid entry in the TCA cycle, while a downregulation of GDH function has been demonstrated for another mitochondrial sirtuin, namely Sirt4 [42,45,46]. Although we did not directly measure the expression of Sirt3 and Sirt4, the observed metabolomic profile suggested a resveratrol-induced increased anaplerotic role of succinate, which is utilised in TCA cycle in association to a decrease in both glycolysis and amino acid utilisation. This hypothesis is supported by the analysis of the pair-wise correlation of succinate; while this metabolite showed no significant correlation with any other metabolite in the control cultures, it acquired a significant positive correlation with lactate in the resveratrol-treated cultures. As succinate is utilised in the Krebs cycle and lactate is released through glycolysis, a positive correlation suggests that when more succinate is utilised, less lactate is produced, in agreement with our experimental data in the treated samples. These results were in agreement with the observation that Sirt3-infected HepG2 cells cultured in the presence of oleate exhibited fewer lipid droplets and significantly more phosphorylation of AMPK and ACC [47].

In conclusion, we have shown that the metabolomic analysis of the exometabolome of resveratrol-treated HepG2 cells indicates a metabolic switch from glucose and amino acid utilisation to fat utilisation for the production of energy. The data presented are consistent with a model in which a resveratrol-induced alteration in glucose utilisation influences SIRT1 and AMPK activity, mimicking calorie restriction, in agreement with several pharmacological and genetic *in vivo* models showing a Sirt1-dependent global shift towards fatty acid oxidation [10,13,37,39,48]. However, considering the multiple cellular targets and different organs distribution, as well as its varying bioavailability and capacity to metabolise resveratrol, it is possible that Sirt1 activation might occur through different mechanisms and pathways, depending on particular conditions [49]. Furthermore, it is now well established that the seven mammalian sirtuin isoforms have different subcellular localisations providing a mechanism of inter-organelle crosstalk, although the specific signalling mechanisms and molecular targets are not yet known. In particular, the increase in succinate utilisation in the Krebs cycle and the correlation of this compound with lactate production observed only in resveratrol-treated cells might suggest an activation of Sirt3 in the mitochondrial subcellular compartment.

Because of the complexity of metabolic interconnections, the effects of resveratrol depend on the biochemical machinery effectively operating in a given subcellular, cellular or organ system.

In this context, a metabolomic approach applied to biological fluids (plasma and urine) could give valuable information on the systemic effects of resveratrol treatment *in vivo* and help to define the most suitable doses and timing of treatment, with the goal of developing a disease-specific personalised intervention.

Supplementary materials related to this article can be found online at doi:10.1016/j.bbagen.2011.10.005.

Acknowledgment

We gratefully acknowledge the help of Dr. Giorgio Capuani for statistical multivariate analysis. The research was supported by a grant from the Italian Ministry of Economy and Finance to the CNR for the Project “FaReBio di Qualita”.

References

[1] J.A. Baur, D. Sinclaie, Therapeutic potential of resveratrol: the in vivo evidence, Nat. Rev. Drug Discov. 5 (2006) 493–506.
[2] C. Alarcón de la Lastra, I. Villegas, Resveratrol as an antioxidant and pro-oxidant agent: mechanism and clinical implications, Biochem. Soc. Trans. 35 (2007) 1156–1160.
[3] F. Brindelli, G. D'Andrea, A. Bozzi, Resveratrol: a natural polyphenol with multiple chemopreventive properties, Curr. Drug Metab. 10 (2009) 530–543.
[4] F.Z. Marquez, M.A. Markus, B.J. Morris, Resveratrol: cellular actions of a potent natural chemical that confers a diversity of health benefits, Int. J. Biochem. Cell Biol. 41 (2009) 2125–2128.
[5] R.F. Guerrero, M.C. Garcia-Pariella, B. Puertas, E. Contos-Villar, Wine, resveratrol and health: a review, Nat. Prod. Commun. 4 (2009) 635–658.
[6] W.R. Leifert, M.J. Abeywardema, Cardioprotective actions of grape polyphenols, Nutr. Res. 28 (2008) 729–737.
[7] M. Pallas, G. Casadesus, M.A. Smith, A. Coto-Montes, C. Palegri, J.J. Villaplana Camins, Resveratrol and neurodegenerative diseases : activation of SIRT-1 as the potential pathway towards neuroprotection, Curr. Neurovasc. Res. 6 (2009) 70–81.
[8] D. Delmas, A. Lancon, D. Collin, B. Jannin, N. La Truffe, Resveratrol as a chemopreventive agent: a promising molecule for fighting cancer, Curr. Drug Targets 7 (2006) 423–442.
[9] M.T. Borra, B.C. Smith, J.M. Denu, Mechanism of human SIRT1 activation by resveratrol, J. Biol. Chem. 280 (2005) 17187–17195.
[10] X. Hou, S. Xu, K.A. Maitland-Toolan, K. Sato, B. Jiang, Y. Ido, F. Lan, K. Walsh, M. WierzBicki, T.J. Verbeuren, R.A. Cohen, M. Zang, SIRT 1 regulates hepatocyte

lipid metabolism through activating AMP-activated protein kinase, J. Biol. Chem. 283 (2008) 20015–20026.
[11] D.M. Taylor, M.M. Maxwell, R. Luthi-Carter, A.G. Kazantsev, Biological and potential therapeutic roles of sirtuin deacetylases, Cell. Mol. Life Sci. 65 (2008) 4000–4018.
[12] J.L. Barger, T. Kayo, J.M. Vann, E.B. Arias, R. Weindruch, T.A. Prolla, A low dose of dietary resveratrol partially mimics caloric restriction and retards aging parameters in mice, PLoS One 3 (2008) e2264.
[13] G.L. Wang, J.C. Fu, W.C. Xu, Y.Q. Feng, S.R. Fang, X.H. Zhou, Resveratrol inhibits the expression of SREB1 in cell model of steatosis via Sirt1-FOXO1 signaling pathway, Biochem. Biophys. Res. Commun. 380 (2009) 644–649.
[14] G. Suchankova, L.E. Nelson, Z. Gerhart-Hines, M. Kelly, M.-S. Gauthier, A.K. Saha, Y. Ido, P. Puigserver, N.B. Ruderman, Concurrent regulation of AMP-activated protein kinase and SIRT1 in mammalian cells, Biochem. Biophys. Res. Commun. 378 (2009) 836–841.
[15] G.S. Oh, H.O. Pae, H. Oh, S.G. Hong, I.K. Kim, K.Y. Chai, Y.G. Yun, T.O. Kwon, H.T. Chung, In vitro antiproliferative effect of 1,2,3,4,6-penta-O-galloyl-beta-D-glucose on human hepatocellular carcinoma cell line, SK-HEP-1 cells, Cancer Lett. 174 (2001) 17–24.
[16] A. Lancon, N. Hanet, B. Jannin, D. Delmas, J.M. Heidel, G. Lizard, M.C. Chagnon, Y. Artur, N. Latruffe, Resveratrol in human hepatoma HepG2 cells: metabolism and inducibility of detoxifying enzymes, Drug Metab. Dispos. 35 (2007) 699–703.
[17] P.L. Kuo, L.C. Chiang, C.C. Lin, Resveratrol-induced apoptosis is mediated by p53-dependent pathway in HepG2 cells, Life Sci. 72 (2002) 23–34.
[18] D. Colin, A. Lancon, D. Delmas, G. Lizard, J. Abrossinow, E. Kahn, B. Jannin, N. Latruffe, Antiproliferative activities of resveratrol and related compounds in human hepatocyte derived HepG2 cells are associated with biochemical cell disturbance revealed by fluorescence analyses, Biochimie 90 (2008) 1674–1684.
[19] A. Tomassini Miccheli, A. Miccheli, R. Di Clemente, M. Valerio, P. Coluccia, M. Bizzarri, F. Conti, NMR-based metabolic profiling of human hepatoma cells in relation to cell growth by culture media analysis, Biochim. Biophys. Acta 1760 (2006) 1723–1731.
[20] J.K. Nicholson, P.J. Foxall, M. Spraul, R.D. Farrant, J.C. Lindon, 750 MHz 1H and 1H-13C NMR spectroscopy of human blood plasma, Anal. Chem. 67 (1995) 793–811.
[21] T.W.-M. Fan, A.N. Lane, Structure-based profiling of metabolites and isotopomers by NMR, Prog. Nuclear Magn. Res. Spect. 52 (2008) 69–117.
[22] L. Eriksson, E. Johansson, N. Kettaneh Wold, S. Wold, Multi and Megavariate Data Analysis, Umetrics AB, Umea, 2001.
[23] A. Miccheli, A. Tomassini, C. Puccetti, M. Valerio, G. Peluso, F. Tuccillo, M. Calvani, C. Manetti, F. Conti, Metabolic profiling by ^{13}C NMR spectroscopy: [1,2-$^{13}C_2$] glucose reveals a heterogeneous metabolism in human leukemia T cells, Biochimie 88 (2006) 437–448.
[24] K.J. Pearson, J.A. Baur, K.N. Lewis, L. Peshkin, N.I. Price, N. Labinsky, W.R. Swindell, D. Kamara, R.K. Minor, E. Perez, H.A. Jamieson, Y. Zhang, S.R. Dunn, K. Sharma, N. Pleshko, L.A. Woollett, A. Csiszar, Y. Ikeno, D. Le Couter, P.J. Elliott, K.G. Beekur, P. Neras, D.K. Ingram, N.S. Wolf, Z. Ungrari, D.A. Sinclair, R. de Cabo, Resveratrol delays age-related deteriration and mimics transcriptional aspects of dietary restriction without extending life span, Cell Metab. 8 (2008) 157–168.
[25] A.L. Holme, S. Pervaiz, Resveratrol in cell fate decision, J. Bioenerg. Biomembr. 39 (2007) 59–63.
[26] J.-L. Beaudeux, V. Nivet-antoine, P. Giral, Resveratrol: a relevant pharmacological approach for the treatment of metabolic syndrome? Curr. Opin. Clin. Nutr. Metab. Care 13 (2010) 729–736.
[27] D.B. Kell, M. Brown, H.M. Davey, W.B. Dunn, I. Spasic, S.G. Oliver, Metabolic footprinting and systems biology: the medium is the message, Nat. Rev. Microbiol. 3 (2005) 557–565.
[28] R. Zhou, M. Fukui, H.J. Choi, B.T. Zhu, Induction of a reversible, non-cytotoxic S-phase delay by resveratrol: implications for a mechanism of lifespan prolongation and cancer protection, Br. J. Pharmacol. 158 (2009) 462–474.
[29] U. Stervbo, O. Vang, C. Bonnessen, Time- and concentration-dependent effects of resveratrol in HL-60 and HepG2 cells, Cell Prolif. 39 (2006) 479–493.
[30] G. Notas, A.P. Nifli, M. Kampa, J. Vercauteren, E. Kouroumalis, E. Castanas, Resveratrol exerts its antiproliferative effect on HepG2 hepatocellular carcinoma cells, by inducing cell cycle arrest, and NOS activation, Biochim. Biophys. Acta 1760 (2006) 1657–1666.
[31] W. Jager, A. Gruber, B. Giessrigl, G. Krupitza, T. Szekeres, D. Sonntag, Metabolomic analysis of resveratrol-induced effects in the human breast cancer cell lines MCF-7 and MDA-MB-231, Omics 15 (2011) 9–14.
[32] A. Kueck, A.W. Opipari Jr., K.A. Griffith, L. Tan, M. Choi, J. Huang, H. Wahl, J.R. Liu, Resveratrol inhibits glucose metabolism in human ovarian cancer cells, Gynecol. Oncol. 107 (2007) 450–457.
[33] A.C. Faber, F.J. Dufort, D. Blair, D. Wagner, M.F. Roberts, T.C. Chiles, Inhibition of phospahatidylinositol 3-kinase-mediated glucose metabolism coincides with resveratrol-induced cell cycle arrest in human diffuse large B-cell lymphomas, Biochem. Pharmacol. 72 (2006) 1246–1256.
[34] D.G. Hardie, Sensing of energy and nutrients by AMP-activated protein kinase, Am. J. Clin. Nutr. 93 (2011) 891S–896S.
[35] N. Ruderman, M. Prentki, AMP kinase and malonyl-CoA: targets for therapy of the metabolic syndrome, Nat. Rev. Drug Discov. 3 (2004) 340–351.
[36] J.T. Rodgers, C. Lerin, W. Haas, S.P. Gygi, B.M. Spiegelman, P. Puigserver, Nutrient control of glucose homeostasis through a complex of PGC-1α and SIRT1, Nature 434 (2005) 113–118.
[37] J.T. Rodgers, P. Puigserver, Fasting-dependent glucose and lipid metabolic response through hepatic sirtuin 1, PNAS 104 (2007) 12861–12866.
[38] J.T. Rodgers, C. Lerin, Z. Gerhart-Hines, P. Puigserver, Metabolic adaptations through the PGC-1α and SIRT1 pathways, FEBS Lett. 582 (2008) 46–53.
[39] B. Ponugoti, D.-H. Kim, Z. Xiao, Z. Smith, J. Miao, M. Zang, S.-Y. Wu, C.-M. Chiang, T.D. Veenstra, J.K. Kemper, SIRT1 deacetylates and inhibits SREBP-1C activity in regulation of hepatic lipid metabolism, J. Biol. Chem. 285 (2010) 33959–33970.
[40] B. Zschoerning, U. Mahlknecht, Sirtuin 1: regulating the regulator, Biochem. Biophys. Res. Commun. 375 (2010) 251–255.
[41] D.J. Lomb, G. Laurent, M.C. Haigis, Sirtuins regulate key aspects of lipid metabolism, Biochim. Biophys. Acta 1804 (2010) 1652–1657.
[42] E. Verdin, M.D. Hirschey, L.W.S. Finley, M.C. Haigis, Sirtuin regulation of mitochondria: energy production, apoptosis, and signaling, Trends Biochem. Sci. 35 (2010) 669–675.
[43] E. Michishita, J.Y. Park, J.M. Burneskis, J.C. Barrett, I. Horikawa, Evolutionarily conserved and nonconserved cellular localizations and functions of human SIRT proteins, Mol. Biol. Cell. 16 (2005) 4623–4635.
[44] C. Schlicker, M. Gertz, P. Papatheodorou, B. Kachholz, C.F. Becker, C. Steegborn, Substrates and regulation mechanisms for the human mitochondrial sirtuins Sirt3 and Sirt5, J. Mol. Biol. 382 (2008) 790–801.
[45] H. Cimen, M.-J. Han, Y. Yang, Q. Tong, H. Koc, E.C. Koc, Regulation of succinate dehydrogenase activity by SIRT3 in mammalian mitochondria, Biochemistry 49 (2010) 304–311.
[46] M.C. Haigis, R. Mostoslavsky, K.M. Haigis, K. Fahie, D.C. Christodoulou, A.J. Murphy, D.M. Valenzuela, G.D. Yancopoulos, M. Karow, G. Blander, C. Wolberger, T.A. Prolla, R. Weindruch, F.W. Alt, L. Guarente, SIRT4 inhibits glutamate dehydrogenase and opposes the effects of calorie restriction in pancreatic beta cells, Cell 126 (2006) 941–954.
[47] T. Shi, G.Q. Fan, S.D. Xiao, SIRT3 reduces lipid accumulation via AMPK activation in human hepatic cells, J. Dig. Dis. 11 (2010) 55–62.
[48] Z. Gerhart-Hines, J.T. Rodgers, O. Bare, C. Lerin, S.-H. Kim, R. Mostoslavsky, F.W. Alt, Z. Wu, P. Puigserver, Metabolic control of muscle mitochondrial function and fatty acid oxidation trough SIRT1/PGC-1α, EMBO J. 26 (2007) 1913–1923.
[49] J.A. Baur, Biochemical effects of SIRT1 activators, Biochim. Biophys. Acta 1804 (2010) 1626–1634.